JACS
JOURNAL OF THE AMERICAN CHEMICAL SOCIETY
Article
pubs.acs.org/JACS

Influence of Backbone Fluorination in Regioregular Poly(3-alkyl-4-fluoro)thiophenes

Zhuping Fei,[†] Pierre Boufflet,[†] Sebastian Wood,[‡] Jessica Wade,[‡] John Moriarty,[§] Eliot Gann,[∥,⊥] Erin L. Ratcliff,[#] Christopher R. McNeill,[∥] Henning Sirringhaus,[§] Ji-Seon Kim,[‡] and Martin Heeney*[,†]

[†]Department of Chemistry and Centre for Plastic Electronics, Imperial College London, Exhibition Rd, London SW7 2AZ, U.K.
[‡]Department of Physics and Centre for Plastic Electronics, Imperial College London, Exhibition Rd, London SW7 2AZ, U.K.
[§]Cavendish Laboratory, University of Cambridge, J J Thomson Avenue, Cambridge CB3 0HE, U.K.
[∥]Department of Materials Science and Engineering, Monash University, Clayton, Victoria 3800, Australia
[⊥]Australian Synchrotron, 800 Blackburn Road, Clayton, Victoria 3168, Australia
[#]Department of Materials Science and Engineering, University of Arizona, Tucson, Arizona 85721, United States

Supporting Information

ABSTRACT: We report two strategies toward the synthesis of 3-alkyl-4-fluorothiophenes containing straight (hexyl and octyl) and branched (2-ethylhexyl) alkyl groups. We demonstrate that treatment of the dibrominated monomer with 1 equiv of alkyl Grignard reagent leads to the formation of a single regioisomer as a result of the pronounced directing effect of the fluorine group. Polymerization of the resulting species affords highly regioregular poly(3-alkyl-4-fluoro)-thiophenes. Comparison of their properties to those of the analogous non-fluorinated polymers shows that backbone fluorination leads to an increase in the polymer ionization potential without a significant change in optical band gap. Fluorination also results in an enhanced tendency to aggregate in solution, which is ascribed to a more co-planar backbone on the basis of Raman and DFT calculations. Average charge carrier mobilities in field-effect transistors are found to increase by up to a factor of 5 for the fluorinated polymers.

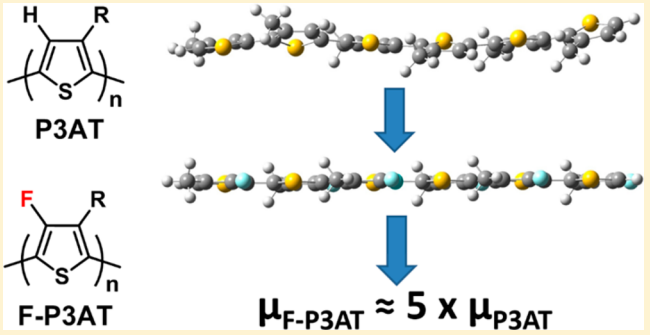

INTRODUCTION

Poly(3-alkyl)thiophenes (P3ATs), in particular poly(3-hexyl)-thiophene (P3HT), are some of the most widely investigated conjugated polymers yet reported.[1] P3HT has been shown to be a promising p-type semiconductor in field-effect transistors (FETs)[2] and exhibits a high efficiency as the donor polymer in organic photovoltaic cells, in particular in blends with substituted fullerene derivatives.[3] The regiochemistry of the solubilizing side chains has been demonstrated to be of particular importance in both of these applications, as it influences the ability of the polymer to aggregate in the solid state.[4] From a synthetic viewpoint the chemistry of P3HT and associated P3ATs is well established,[5] with readily scalable routes reported for the synthesis of regioregular polymer.[6] This is particularly important for applications in which cost of the semiconductor will be an important factor, such as solar cells. Routes to carefully control and manipulate the polymer end group are also established,[7] and P3ATs have been shown to exhibit chain growth polymerization with living character,[8] enabling the synthesis of more complex block co-polymers.[9] Although this combination of properties makes P3ATs potentially attractive for many large-scale applications, there are drawbacks in terms of performance in devices. Principally in the case of FETs, the small ionization potential of P3AT, as a result of its electron rich backbone, can lead to issues with ambient stability, due to expeditious doping by atmospheric oxygen and/or water.[10] For solar cells, the small ionization potential results in rather low open-circuit voltages limiting efficiency.[11] Hence, synthetic manipulations to improve the intrinsic properties of P3AT, while maintaining the simple and scalable polymerization chemistries, are of high potential interest.

Most routes to modify P3AT properties have focused upon co-polymerization with a range of co-monomers to influence the optoelectronic properties.[12] Other efforts have focused upon manipulation of the heteroatom, for example changing from thiophene to furan,[13] selenophene[14] or tellurophene[15] has been shown to significantly influence the properties of the resulting regioregular homo-polymers. However, there has been less focus on the manipulation of the P3AT backbone itself, probably because the incorporation of substituents into the vacant 4-position of the thiophene can lead to undesirable steric interactions with adjacent monomers, and therefore twisting of

Received: March 17, 2015
Published: May 21, 2015

DOI: 10.1021/jacs.5b02785
J. Am. Chem. Soc. 2015, 137, 6866−6879

the backbone out of conjugation. For example, bromination of the polymer backbone leads to a significant blue-shift in absorption as a result of this twisting caused by the large steric bulk of the bromo substituent.[16] We were interested to investigate the properties of fluorinated analogues of P3AT, in which the polymer backbone itself was fluorinated (we note that side-chain-fluorinated P3ATs have been previously reported[17]). Due to the relatively small size of fluorine, we expected that disruptive steric interactions with adjacent 3-alkylthiophenes would be minimized, while the strong electron-withdrawing nature of fluorine should result in an increase in ionization potential. In addition, fluorine's unusual combination of being strongly inductively withdrawing while mesomerically donating is known to exert a significant influence on inter- and intramolecular packing in the solid state.[18] The exact role of the F atom in solid-state morphology is complex, although intra- and intermolecular interactions between S and F atoms have been suggested in some instances.[19]

There have been relatively few examples of either oligomeric or polymeric materials containing fluorinated thiophene. This paucity is probably related to the synthetic complexity of obtaining fluorinated thiophene building blocks.[20] Perfluorinated thiophene oligomers from the trimer to the hexamer have been reported by Suzuki and co-workers.[21] Fluorination was shown to reduce intermolecular distances within the single crystal in comparison to non-fluorinated polymers. Poly(3-fluorothiophene) has been synthesized electrochemically as an insoluble material displaying a higher oxidation potential than polythiophene,[22] while more recently the electropolymerization of a singly fluorinated terthiophene derivative has been reported.[23] Co-polymers of 3-fluorothiophene or 3,4-difluorothiophene in combination with solubilizing co-monomers have also been reported as possible transistor and solar cell polymer materials.[24]

In this work we report the synthesis, properties, characterization, and OFET performance of regioregular poly(3-alkyl-4-fluorothiophenes) with branched and straight alkyl side chains, and compare these with their non-fluorinated counterparts. We observe significant differences in the physical behavior of the polymers, with backbone fluorination leading to an increase in melting enthalpy and temperature, and a reduction in solubility. These observations are rationalized by density functional theory (DFT) calculations on hexameric oligomers, which suggest a planarization of the polymer backbone upon fluorination. Differences in the observed Raman spectra of thin films support significant differences in backbone planarization. We also observe notable increases in the polymer ionization potential upon fluorination. Finally FET devices are fabricated, demonstrating that backbone fluorination has a sizable beneficial impact on charge transport.

EXPERIMENTAL SECTION

General. Reagents and chemicals were purchased from commercial sources such as Aldrich and Acros etc. unless otherwise noted. 3-(2-Ethylhexyl)thiophene (**1c**), 2,3,5-tribromo-4-hexylthiophene (**2a**), 2,3,5-tribromo-4-octylthiophene (**2b**), 3-bromo-4-hexyl-2,5-bis-(trimethylsilyl)thiophene (**3a**), 3-fluoro-4-hexyl-2,5-bis(trimethylsilyl)-thiophene (**4a**), 2,5-dibromo-3-fluoro-4-hexylthiophene (**5a**), and 2,5-bis(trimethylsilyl)-3,4-dibromothiophene (**7**) were synthesized by the reported methods.[23,25]

All reactions were carried out under argon using solvents and reagents as commercially supplied, unless otherwise stated. *N*-Fluorobenzenesulfonimide (NFSI) was dried overnight under high vacuum before use. ^{1}H, ^{19}F, and ^{13}C NMR spectra were recorded on a Bruker AV-400 (400 MHz), using the residual solvent resonance of $CDCl_3$, *o*-DCB-d_4, or d_2-1,1,2,2-tetrachloroethene, and values are given in ppm. Number-average (M_n) and weight-average (M_w) molecular weights were determined by using an Agilent Technologies 1200 series Gel permeation chromatography (GPC) running in chlorobenzene at 80 °C, using two PL mixed B columns in series, and calibrated against narrow-polydispersity polystyrene standards. Preparative Gel permeation chromatography utilized a Shimadzu recycling GPC system running in hexane at 40 °C or chlorobenzene at 80 °C, using Agilent PLgel 10 μm 50A or MIXED-D column, DGU-20A3 degasser, LC-20A pump, CTO-20A column oven, and SPD-20A UV detector. Electrospray mass spectrometry was performed with a Thermo Electron Corp. DSQII mass spectrometer. UV−vis spectra were recorded on a UV-1601 Shimadzu UV−vis spectrometer. Flash chromatography (FC) was performed on silica gel (Merck Kieselgel 60 F254 230−400 mesh) or using a Biotage SNAP cartridge (KP-C18-HS, 120 g) on a Biotage Isolera instrument. Photoelectron spectroscopy in air (PESA) measurements were recorded with a Riken Keiki AC-2 PESA spectrometer with a power setting of 5 nW and a power number of 0.5. Samples for PESA were prepared on glass substrates by spin-coating. Differential scanning calorimetry (DSC) measurements, using ∼3 mg of material, were conducted under nitrogen at scan rate of 10 °C/min with a TA DSC-Q20 instrument. Films for Raman, GIWAXS, and ultraviolet photoemission spectroscopy (UPS) measurements were prepared by spin-coating from hot (ca. 150 °C) solution in 1,2,4-trichlorobenzene (TCB, 10 mg/mL) at 3000 rpm for F-P3OT and room-temperature TCB for P3OT. Films for F-P3EHT and P3EHT were prepared from chloroform.

Grazing-incidence wide-angle X-ray scattering (GIWAXS) measurements were performed at the SAXS/WAXS beamline at the Australian Synchrotron,[26] using 9 keV photons. 2D scattering patterns were recorded by using a Dectris Pilatus 1M detector. The sample-to-detector distance was calibrated using a silver behenate standard. Scattering patterns were recorded as a function of X-ray angle of incidence, with the angle of incidence varied from 0.05° below the critical angle of the organic film to 0.2° above the critical angle. The images reported were just above the critical angle, as identified by the angle with the highest scattering intensity. Data acquisition times of 3 s were used, with three 1 s exposures taken with offset detector positions to cover gaps in the Pilatus detector. X-ray diffraction data are expressed as a function of the momentum transfer in the directions perpendicular to and parallel to the plane of the sample, q_z and q_{xy}, respectively, which have a magnitude of $(4\pi/\lambda)\sin(\theta)$, where θ is half the corresponding scattering angle and λ is the wavelength of the incident radiation.

Raman spectra were measured using a Renishaw inVia Raman spectrometer with 785 nm diode laser excitation. Laser power at the sample was 130 mW, focused to a 40 μm^2 area. The photoluminescence background was subtracted from the spectra using a polynomial baseline, and then the spectra were normalized to the main peak. A Linkam THMS600 hot−cold cell purged with nitrogen was used to prevent polymer degradation as well as to control the temperature of the sample. For room-temperature measurements, the total laser exposure time was 25 s, whereas the exposure time for temperature-dependent spectra was 10 s. Starting from room temperature, the sample was heated at 10 °C/min to 300 or 410 °C and then held for 10 min before cooling at 10 °C/min. The temperature was held for 1 min at every 10 °C interval in order to measure spectra.

DFT calculations were carried out using the B3LYP hybrid functional and the 6-31G* basis set in the GAUSSIAN09 software package.[27] Alkyl chains were replaced with a methyl group to simplify calculations and reduce computational time. Structures were first optimized, and then a frequency analysis was used to simulate Raman activities in order to identify the Raman-active vibrational modes. Potential energy scans were performed upon hexamers using the redundant coordinate editor and scanning the central dihedral angle in 36 steps of 10° increments.

FETs were fabricated on low-sodium glass with an interdigitated electrode structure with a channel length and width of 20 μm and 1

DOI: 10.1021/jacs.5b02785
J. Am. Chem. Soc. 2015, 137, 6866−6879

mm, respectively. Electrodes were fabricated from gold via photolithography. Active layers were deposited via zone casting (5 mg/mL solutions in 1,2-dichlorobenzene), solution temperature of 140 °C, followed by thermal annealing at 140 °C. The process was performed in nitrogen. For devices fabricated with P3HT, P3OT, and their fluorinated variants, electronic-grade poly(methyl methacrylate) (PMMA) dissolved in anhydrous *n*-butyl acetate (45 mg mL^{-1}) was spin-coated onto the films (PMMA thickness ≈ 550 nm). For P3EHT and F-P3EHT, CYTOP (500 nm) was used as the dielectric layer. Following dielectric deposition, the devices were thermally annealed again (90 °C for 30 min). In the final step, gold contact electrodes were evaporated through a shadow mask to complete the devices. Devices were characterized in nitrogen using an Agilent 4155B semiconductor parameter analyzer.

Synthesis of 2,3,5-Tribromo-4-(2-ethylhexyl)thiophene (2c). Br_2 (12.5 mL, 244 mmol) was added dropwise to a solution of 3-(2-ethylhexyl)thiophene (16 g, 81 mmol) in acetic acid (100 mL) in the absence of light. After the addition of bromine, the mixture was stirred at room temperature for 2 h and heated to 60 °C overnight. The mixture was poured into ice water (300 mL) and neutralized with 5 M NaOH solution. The mixture was extracted by hexane (3 × 100 mL). The combined organics were washed by brine (2 × 200 mL) and water (2 × 200 mL), dried ($MgSO_4$), and filtered, and the solvent was removed under reduced pressure. The residue was purified by silica gel chromatography (eluent: petroleum ether 40−60 °C) to afford **2c** as a pale yellow oil (28.6 g, yield: 81%). ^{1}H NMR (400 MHz, $CDCl_3$) δ (ppm): 2.57 (d, J = 7.3 Hz, 2H), 1.77−1.68 (m, 1H), 1.36−1.21 (m, 8H), 0.92−0.88 (m, 6H). ^{13}C NMR ($CDCl_3$, 100 MHz) δ (ppm): 140.8, 116.3, 109.6, 109.0, 38.9, 35.3, 32.5, 28.8, 25.7, 23.1, 14.2, 11.0. HRMS (EI+) calcd for $C_{12}H_{17}Br_3S$: 429.8601; found: 429.8615.

Synthesis of 3-Bromo-4-octyl-2,5-bis(trimethylsilyl)-thiophene (3b). A solution of *n*-BuLi (29.1 mL of a 2.5 M solution in hexanes, 72.7 mmol) was added dropwise to a solution of **2b** (15 g, 34.6 mmol) in tetrahydrofuran (THF, 100 mL) at −78 °C. After the solution was stirred for 15 min at −78 °C, chlorotrimethylsilane (9.7 mL, 76 mmol) was added in one portion. The cooling bath was removed, and the reactant was allowed to warm to room temperature, followed by stirring for 0.5 h at room temperature. Water (100 mL) was added, and the mixture was extracted (3 × 100 mL hexane). The combined organics were dried ($MgSO_4$), filtered, and concentrated under reduced pressure. The residue was purified by silica gel chromatography (eluent: petroleum ether 40−60 °C) to afford **3b** as a pale yellow oil (12.8 g, yield: 88%). ^{1}H NMR (400 MHz, $CDCl_3$) δ (ppm): 2.67−2.63 (m, 2H), 1.54−1.50 (m, 2H), 1.37−1.28 (m, 10H), 0.88 (t, J = 6.9 Hz, 3H), 0.38 (s, 9H), 0.33 (s, 9H). ^{13}C NMR ($CDCl_3$, 100 MHz) δ (ppm): 150.1, 139.2, 138.8, 121.7, 31.9, 31.1, 30.9, 30.1, 29.4, 29.3, 22.7, 14.2, 0.1, −0.8. HRMS (EI+) calcd for $C_{18}H_{35}BrSSi_2$: 418.1181; found: 418.1181.

Synthesis of 3-Bromo-4-(2-ethylhexyl)-2,5-bis-(trimethylsilyl)thiophene (3c). A solution of *n*-BuLi (37.2 mL of a 2.5 M solution in hexanes, 93 mmol) was added dropwise to a solution of **2c** (19.2 g, 44.3 mmol) in THF (100 mL) at −78 °C. After the solution was stirred for 15 min at −78 °C, chlorotrimethylsilane (12.4 mL, 98 mmol) was added in one portion. The cooling bath was removed, and the reactant was allowed to warm to room temperature, followed by stirring for 0.5 h at room temperature. Water (100 mL) was added, and the mixture was extracted (3 × 100 mL hexane). The combined organics were dried ($MgSO_4$), filtered, and concentrated under reduced pressure. The residue was purified by silica gel chromatography (eluent: petroleum ether 40−60 °C) to afford **3c** as a pale yellow oil (15.3 g, yield: 82%). ^{1}H NMR (400 MHz, $CDCl_3$) δ (ppm): 2.65 (d, J = 7.6 Hz, 2H), 1.82−1.76 (m, 1H), 1.27−1.21 (m, 8H), 0.89−0.83 (m, 6H), 0.39 (s, 9H), 0.35 (s, 9H). ^{13}C NMR ($CDCl_3$, 100 MHz) δ (ppm): 148.9, 139.8, 139.1, 122.3, 39.7, 35.3, 32.8, 29.0, 26.1, 23.1, 14.1, 11.3, 0.7, −0.8. HRMS (EI) [M + H] calcd for $C_{18}H_{36}BrSSi_2$: 419.1260; found: 419.1270.

Synthesis of 3-Fluoro-4-octyl-2,5-bis(trimethylsilyl)-thiophene (4b). A solution of *n*-BuLi (6.3 mL of a 2.5 M solution in hexanes, 15.7 mmol) was added dropwise to a solution of of **3b** (6.0 g, 14.3 mmol) in THF (200 mL) at −78 °C. After the solution was stirred for 15 min at −78 °C, NFSI (4.9 g, 17.2 mmol) in THF (50 mL) was slowly added, and the solution was stirred for 2 h at −78 °C and then overnight with warming to room temperature. Water (100 mL) was added, and the mixture was extracted (3 × 100 mL hexane). The combined organics were dried ($MgSO_4$), filtered, and concentrated under reduced pressure. The residue was purified by silica gel chromatography (eluent: petroleum ether 40−60 °C) to afford a pale yellow oil (2.7 g, yield: 52%). ^{1}H NMR (400 MHz, $CDCl_3$) δ (ppm): 2.58−2.54 (m, 2H), 1.59−1.51 (m, 2H), 1.38−1.29 (m, 10H), 0.88 (t, J = 6.9 Hz, 3H), 0.34 (s, 9H), 0.33 (s, 9H). ^{13}C NMR ($CDCl_3$, 100 MHz) δ (ppm): 163.4 (d, J = 261 Hz), 139.1 (d, J = 24 Hz), 138.5, 122.0 (d, J = 30 Hz), 31.9, 30.8, 29.9, 29.4, 29.3, 28.2, 22.7, 14.1, −0.1, −0.5. ^{19}F NMR ($CDCl_3$) δ (ppm): −122.0. HRMS (EI+) calcd for $C_{18}H_{35}FSSi_2$: 358.1982; found: 358.1989.

Synthesis of 3-Fluoro-4-(2-ethylhexyl)-2,5-bis-(trimethylsilyl)thiophene (4c). A solution of *n*-BuLi (8.5 mL of a 2.5 M solution in hexanes, 21.3 mmol) was added dropwise to a solution of **3c** (8.1 g, 19.3 mmol) in THF (200 mL) at −78 °C. After the solution was stirred for 15 min at −78 °C, NFSI (6.6 g, 23.2 mmol) in THF (60 mL) was slowly added, and the solution was stirred for 2 h at −78 °C and then overnight with warming to room temperature. Water (100 mL) was added, and the mixture was extracted (3 × 100 mL hexane). The combined organics were dried ($MgSO_4$), filtered, and concentrated under reduced pressure. The residue was purified by silica gel chromatography (eluent: petroleum ether 40−60 °C) to afford a pale yellow oil (3.2 g, yield: 46%). ^{1}H NMR (400 MHz, $CDCl_3$) δ (ppm): 2.50 (d, J = 7.5 Hz, 2H), 1.65−1.61 (m, 1H), 1.28−1.17 (m, 8H), 0.90−0.84 (m, 6H), 0.32 (s, 9H), 0.31 (s, 9H). ^{13}C NMR ($CDCl_3$, 100 MHz) δ (ppm): 164.9 (d, J = 260 Hz), 139.3, 138.2 (d, J = 24 Hz), 119.3 (d, J = 30 Hz), 39.8, 32.7, 32.7, 28.8, 26.0, 23.0, 14.0, 11.0, 0.2, −0.6. ^{19}F NMR ($CDCl_3$) δ (ppm): −119.5. HRMS (EI) [M + H] calcd for $C_{18}H_{36}FSSi_2$: 359.2060; found: 359.2051.

Synthesis of 2,5-Dibromo-3-fluoro-4-octylthiophene (5b). A solution of Br_2 (0.79 mL, 15.3 mmol) in CH_2Cl_2 (10 mL) was added dropwise to a solution of **4b** (2.5 g, 7.0 mmol) in CH_2Cl_2 (50 mL) at 0 °C in the absence of light. The reaction was allowed to warm to room temperature and stirred for 2 h. A saturated sodium sulfite solution (20 mL) was added. The aqueous phase was extracted with CH_2Cl_2 (2 × 30 mL). The combined organic phase was dried ($MgSO_4$), filtered, and concentrated under reduced pressure. The residue was purified by silica gel chromatography (eluent: petroleum ether 40−60 °C), followed by preparative GPC in hexane to afford **5b** as a colorless oil (2.2 g, yield: 86%). ^{1}H NMR (400 MHz, $CDCl_3$) δ (ppm): 2.52 (m, 2H), 1.59−1.44 (m, 2H), 1.30- 1.27 (m, 10H), 0.88 (t, J = 6.9 Hz, 3H). ^{13}C NMR ($CDCl_3$, 100 MHz) δ (ppm): 153.5 (d, J = 264 Hz), 132.3 (d, J = 23 Hz), 107.4 (d, J = 10 Hz), 89.4 (d, J = 23 Hz), 31.9, 29.3, 29.2, 29.1, 28.5, 27.1, 22.7, 14.1. ^{19}F NMR ($CDCl_3$) δ (ppm): −124.2. HRMS (EI+) calcd for $C_{12}H_{17}Br_2FS$: 369.9402; found: 369.9412.

Synthesis of 2,5-Dibromo-3-fluoro-4-(2-ethylhexyl)-thiophene (5c). A solution of Br_2 (0.72 mL, 14.1 mmol) in CH_2Cl_2 (10 mL) was added dropwise to a solution of **4c** (2.5 g, 7.0 mmol) in CH_2Cl_2 (50 mL) at 0 °C in the absence of light. The reactant was then allowed to warm to room temperature and stirred for 2 h. A saturated sodium sulfite solution (20 mL) was added. The aqueous phase was extracted with CH_2Cl_2 (2 × 30 mL). The combined organic phase was dried ($MgSO_4$), filtered, and concentrated under reduced pressure. The residue was purified by silica gel chromatography, (eluent: petroleum ether 40−60 °C), followed by preparative GPC in hexane to afford **5c** as a colorless oil (1.98 g, yield: 83%). ^{1}H NMR (400 MHz, $CDCl_3$) δ (ppm): 2.43 (d, J = 7.5 Hz, 2H), 1.63−1.58 (m, 1H), 1.31−1.18 (m, 8H), 0.90−0.82 (m, 6H). ^{13}C NMR ($CDCl_3$, 100 MHz) δ (ppm): 153.6 (d, J = 264 Hz), 131.8 (d, J = 23 Hz), 107.9 (d, J = 10 Hz), 89.3 (d, J = 23 Hz), 31.9, 29.3, 29.2, 29.1, 28.5, 27.1, 22.7, 14.1. ^{19}F NMR ($CDCl_3$) δ (ppm): −123.2. HRMS (EI+) calcd for $C_{12}H_{17}Br_2FS$: 369.9402; found: 369.9393.

Synthesis of 2,5-Bis(trimethylsilyl)-3-bromo-4-fluorothiophene (8). A solution of *t*-BuLi (8.0 mL of a 1.7 M solution in pentane, 13.6 mmol) was added dropwise to a solution of 7 (5.0 g, 13

DOI: 10.1021/jacs.5b02785
J. Am. Chem. Soc. 2015, 137, 6866−6879

Scheme 1. Synthetic Route A to Monomers and Polymers

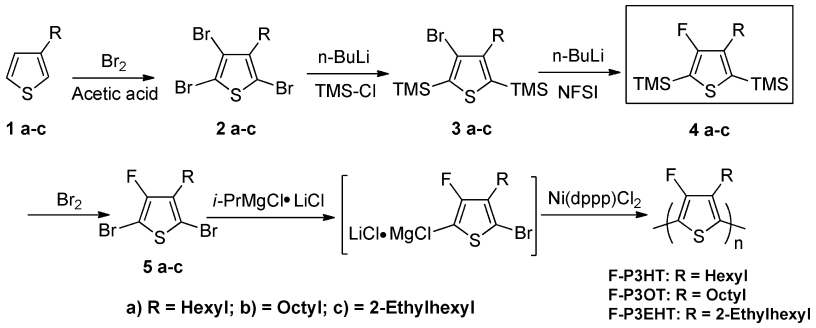

mmol) in diethyl ether (150 mL) at −78 °C. After the solution was stirred for 10 min at −78 °C, NFSI (4.22 g, 14.9 mmol) in THF (7 mL) was added dropwise, and the solution was stirred for 2 h at this temperature and then overnight with warming to room temperature. Water (100 mL) was added, and the mixture was extracted (3 × 100 mL diethyl ether). The combined organics were dried ($MgSO_4$), filtered, and concentrated under reduced pressure. The residue was purified by reverse-phase chromatography (eluent: methanol) to afford a colorless oil (2.1 g, yield: 50%). ^{1}H NMR (400 MHz, $CDCl_3$) δ (ppm): 0.39 (s, 9H), 0.33 (s, 9H). ^{13}C NMR ($CDCl_3$, 100 MHz) δ (ppm): 160.1 (d, J = 260 Hz), 139.6, 120.5 (d, J = 30 Hz), 107.7 (d, J = 30 Hz), −0.8, −1.3. ^{19}F NMR ($CDCl_3$) δ (ppm): −117.7. HRMS (EI) + calcd for $C_{10}H_{18}BrFSSi_2$: 323.9835; found: 323.9830.

Synthesis of 3-Fluoro-4-octyl-2,5-bis(trimethylsilyl)-thiophene (4b) (Route B). Octylmagnesium bromide (3.33 mL of a 2 M solution in diethyl ether) was added to a stirred solution of zinc chloride (6.66 mL of a 1 M solution in diethyl ether) under argon. The solution was stirred for 30 min before being added to a dry 20 mL high-pressure microwave reactor tube containing **8** (1.67 g, 5.13 mmol) and Pd(dppf)Cl_2 (0.34 g, 0.46 mmol). The tube was sealed, flushed with Ar, and heated overnight at 80 °C (oil bath temperature). After cooling to room temperature, the mixture was passed through a 5 × 5 × 5 cm silicon plug (eluent: hexane), and the organic solvent was concentrated under reduced pressure. The residue was purified by reverse-phase chromatography (eluent: methanol) to afford **4b** as a pale yellow oil (0.79 g, 43%), which exhibited NMR spectra identical to those reported earlier.

Synthesis of 3-Fluoro-4-(2-ethylhexyl)-2,5-bis-(trimethylsilyl)thiophene (4c) (Route B). To a dry 20 mL high-pressure microwave reactor tube were added **8** (1.0 g, 3.1 mmol) and Pd(dppf)Cl_2 (0.11 g, 0.15 mmol). The tube was sealed and flushed with Ar, and then dry, degassed THF (10 mL) and (2-ethylhexyl)zinc bromide (7.4 mL of a 0.5 M solution in THF, 3.7 mmol) were added. The solution was thoroughly degassed under argon, and the reaction was heated overnight at 80 °C (oil bath temperature). After cooling to room temperature, the mixture was passed through a 5 × 5 × 5 cm silicon plug (eluent: hexane), and the organic solvent was concentrated under reduced pressure. The residue was purified by reverse-phase chromatography (eluent: methanol) to afford **4c** as a pale yellow oil (0.34 g, 31%), which exhibited NMR spectra identical to those reported earlier.

Synthesis of Poly[3-fluoro-4-hexylthiophene-2,5-diyl] (F-P3HT). In a three-necked flask, a solution of 2,5-dibromo-3-fluoro-4-hexylthiophene (1.02 g, 2.96 mmol) in anhydrous THF (20 mL) was cooled to 0 °C. A solution of isopropylmagnesium chloride/lithium chloride complex (2.21 mL of a 1.3 M solution in THF, 2.88 mmol) was added via syringe, and the cooling bath was removed. After the mixture was stirred for 30 min at room temperature, the reaction was heated to reflux for 30 min. The heating bath was lowered so that the temperature dropped just below reflux, and the catalyst Ni(dppp)Cl_2 (8.0 mg, 0.015 mmol) in THF (1 mL) was added in one portion. The reaction was refluxed for 4 h and allowed to cool to room temperature. The reaction mixture was precipitated into a well-stirred solution of methanol (40 mL)/25% HCl (10 mL) and stirred for 1 h. The resulting suspension was filtered directly into a Soxhlet thimble. This was extracted (Soxhlet) with methanol, acetone, hexane, chloroform, and chlorobenzene. The chlorobenzene solution was concentrated and precipitated into methanol, and the precipitant was filtered and dried under vacuum to afford a dark solid (167 mg, yield: 30%, rr = 93%). ^{1}H NMR (1,2-dichlorobenzene-d_4, 400 MHz, 130 °C), δ (ppm): 2.99 (broad, 2H), 1.93−1.86 (broad, 2H), 1.58−1.46 (broad, 6H), 1.04 (broad, 3H).

Synthesis of Poly[3-fluoro-4-octylthiophene-2,5-diyl] (F-P3OT). In a three-necked flask, a solution of 2,5-dibromo-3-fluoro-4-octylthiophene (0.82 g, 2.20 mmol) in anhydrous THF (18 mL) was cooled to 0 °C. A solution of isopropylmagnesium chloride/lithium chloride complex (1.65 mL of a 1.3 M solution in THF, 2.14 mmol) was added via syringe, and the cooling bath was removed. After the mixture was stirred for 30 min at room temperature, the reaction was heated to reflux for 30 min. The heating bath was lowered so that the temperature dropped just below reflux, and the catalyst Ni(dppp)Cl_2 (6.0 mg, 0.011 mmol) in THF (1 mL) was added in one portion. The reaction was refluxed for 4 h and allowed to cool to room temperature. The reaction mixture was precipitated into a well-stirred solution of methanol (40 mL)/25%. HCl (10 mL) and stirred for 1 h. The resulting suspension was filtered directly into a Soxhlet funnel. This was extracted (Soxhlet) with methanol, acetone, hexane, chloroform, and chlorobenzene. The chlorobenzene solution was concentrated and precipitated into methanol, and the precipitant was filtered and dried under vacuum to afford a dark solid (210 mg, 44%, M_n = 23K, PDI = 1.8, rr = 96%).^{1}H NMR (1,1,2,2-tetrachloroethane-d_4, 400 MHz, 130 °C), δ (ppm): 2.82 (broad, 2H), 1.75−1.72 (broad, 2H), 1.44−1.37 (broad, 10H), 0.96 (broad, 3H). ^{19}F NMR (1,1,2,2-tetrachloroethane-d_4, 400 MHz, 130 °C) δ (ppm): −123.0.

Synthesis of Poly[3-fluoro-4-(2-ethylhexyl)thiophene-2,5-diyl] (F-P3EHT). In a three-necked flask, a solution of 2, 5-dibromo-3-fluoro-4-(2-ethylhexyl)thiophene (0.86 g, 2.31 mmol) in anhydrous THF (18 mL) was cooled to 0 °C. A solution of isopropylmagnesium chloride/lithium chloride complex (1.72 mL of a 1.3 M solution in THF, 2.24 mmol) was added via syringe, and the cooling bath was removed. After the mixture was for 30 min at room temperature, the reaction was heated to reflux for 30 min. The heating bath was lowered so that the temperature dropped just below reflux, and the catalyst Ni(dppp)Cl_2 (6.2 mg, 0.012 mmol) in THF (1 mL) was added in one portion. The reaction was refluxed for 4 h and allowed to cool to room temperature. The reaction mixture was precipitated into a well-stirred solution of methanol (40 mL)/25% HCl (10 mL) and stirred for 1 h. The resulting suspension was filtered directly into a Soxhlet funnel. This was extracted (Soxhlet) with methanol, acetone, hexane, and chloroform. The chloroform solution was concentrated and precipitated into methanol, and the precipitant was filtered and dried under vacuum to afford a dark solid (307 mg, 62%, M_n = 28K, PDI = 1.3, rr = 96%). ^{1}H NMR (1,1,2,2-tetrachloroethane-d_4, 400 MHz, 130 °C), δ (ppm): 2.68 (broad, 2H), 1.67 (broad, 1H), 1.33−1.24 (broad, 8H), 0.87−0.85 (broad, 6H). ^{19}F NMR (1,1,2,2-tetrachloroethane-d_4, 400 MHz, 130 °C) δ (ppm): −121.6.

DOI: 10.1021/jacs.5b02785
J. Am. Chem. Soc. 2015, 137, 6866−6879

RESULTS AND DISCUSSION

Synthesis and Characterization of Monomers and Polymers. We decided to focus upon the Grignard metathesis (GRIM) route to synthesize the fluorinated polymers, because of the well-known robustness and good control that this route offers for P3HT.[1b] The critical building block was therefore the synthesis of 2,5-dibromo-4-fluoro-3-alkythiophene. Fluorination of electron-rich aromatic thiophenes in the 3,4-positions is non-trivial but has been achieved by the electrophilic fluorination of lithiated thiophenes.[21a] Due to the propensity of the 3- or 4-lithiated thiophenes to rearrange to the more thermodynamically stable 2,5-positions, these positions must be protected prior to reaction. Our initial synthesis route to 2,5-dibromo-3-fluoro-4-alkylthiophene monomers is shown in Scheme 1. A similar synthetic route to **3a** has recently been reported.[23] We investigated two straight-chain derivatives, hexyl and octyl, as well as a branched 2-ethylhexyl derivative.

3-Alkylthiophene was exhaustively brominated by treatment with bromine to afford 2,3,5-tribromo-4-alkylthiophene (**2a**–**2c**) in yields of 81–88%. Subsequent treatment with *n*-BuLi at low temperature, followed by quenching with chlorotrimethylsilane afforded 3-bromo-4-alkyl-2,5-bis(trimethylsilyl)thiophene (**3a**–**3c**) in typical yields of 82–88%. Then 3-fluoro-4-alkylthiophene (**4a**–**4c**) was prepared by lithiation of **3a**–**3c**, followed by addition of *N*-fluorobenzenesulfonimide in yields of 46–52%. The low yields for fluorination reactions are principally attributed to the losses of material during purification. Indeed, the major byproduct of these reactions was the non-fluorinated analogue, which has only a slight difference in retention factor from the product, rendering purification through normal-phase chromatography particularly time-consuming. For that reason, preparative GPC or reverse-phase chromatography was used, the former being particularly effective for separating **5** from **2** (byproduct from the bromination of **4**). Hence, mixtures of **4** containing small amounts of the non-fluorinated byproduct were typically brominated to give a mixture of **5** and **2**, which could be more readily separated. This route affords the monomers in a moderate overall yield of 20–30%.

One difficulty with this initial route was the early-stage introduction of the alkyl side chain, which meant that all four steps needed to be repeated to change the side chain. Due to tedious nature of the separation of the fluorinated monomer from the non-fluorinated byproduct, we designed an alternate synthesis route in which the alkyl side chains are introduced after the fluorination step (Scheme 2). Here, the fluorinated intermediate **8** was made from commercially available 2,3,4,5-tetrabromothiophene in two steps and could be separated from the non-fluorinated byproduct by reverse-phase chromatography in reasonable quantities. Surprisingly, **8** was unreactive to the standard Kumada coupling conditions used for 3-bromothiophene,[28] so alkyl chains were incorporated by Negishi cross-coupling with octyl or 2-ethylhexyl zinc bromide in the presence of $Pd(dppf)Cl_2$ as catalyst. Alkylation yields of the branched side chain were slightly lower than the straight chain analogue (31% and 43%, respectively), presumably due to the larger steric demand of the (2-ethylhexyl)zinc reagent, although a limited number of catalytic systems were screened, so these yields could reasonably be increased.

Scheme 2. Improved Synthetic Route B to Intermediates 4b and 4c

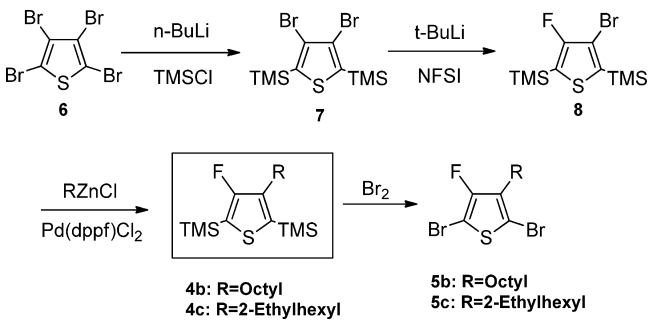

Polymerization was achieved by following a similar method to the GRIM route developed for thiophene polymers.[29] Interestingly the presence of the fluorine substituent has a beneficial impact of the selectivity of the metathesis step. Whereas treatment of 2,5-dibromo-3-octylthiophene with 0.97 equiv of isopropylmagnesium bromide/lithium chloride affords an approximate 4:1 mixture of Grignard isomers in agreement with the literature,[30] reaction of 2,5-dibromo-3-fluoro-4-octylthiophene afforded essentially 100% of a single Grignard isomer (as observed by GCMS of a quenched sample, Supporting Information, Figure S1.). A doublet peak at 6.62 (J = 1.2 Hz) ppm and at −125.9 ppm in ^{1}H and ^{19}F NMR, respectively (Figures S2 and S3), suggested that metathesis had occurred exclusively with the Br which is adjacent to the F atom (as shown in Scheme 1). 2D HOESY NMR (^{1}H and ^{19}F NMR, Figure S4) further confirmed the close spatial proximity of the H and F. No quenched products arising from bis-Grignard formation were detected. The formation of a single isomer of the thienyl Grignard has previously been shown to be beneficial in improving the control of the polymerization,[31] although for the non-fluorinated monomer this was achieved by differentiation of the 2 and 5 positions of the thiophene ring with different halogen substituents.

Addition of $Ni(dppp)Cl_2$ to the hot Grignard solution afforded rapid formation of the polymer F-P3OT. The same procedure was applied to synthesize F-P3HT and F-P3EHT. The crude polymers were purified by a combination of precipitation and Soxhlet extraction to remove low-weight oligomers and catalyst impurities. After removal of impurities the polymers were extracted into chlorobenzene to isolate soluble fractions. The resulting polymers had substantially different solubility compared to their non-fluorinated analogues, and F-P3HT and F-P3OT could only be dissolved in chlorinated aromatic solvents at high temperature. The branched F-P3EHT exhibited improved solubility and could be dissolved in hot chloroform as well as chlorobenzene. The yields of F-P3HT, F-P3OT, and F-P3EHT were 30%, 44%, and 62%, respectively. The low yields of F-P3HT and F-P3OT may be attributed to precipitation of polymer chain from solvent during polymerization progress.[31]

F-P3OT and F-P3EHT had M_n = 23 kDa with $Đ$ = 1.8 and M_n = 28 kDa with $Đ$ = 1.3, respectively (Table 1), as measured by GPC in hot chlorobenzene (80 °C) against polystyrene standards. However, the molecular weight of F-P3HT could not be measured due to its poor solubility. In order to allow for a direct comparison to the fluorinated polymers, similar molecular weight P3OT and P3EHT were prepared by an identical polymerization procedure and fractionated by preparative GPC (chlorobenzene) to obtain comparable molecular weights. The percentage of side-chain regioregularity (rr) was measured by integration of the methylene signals in ^{1}H

DOI: 10.1021/jacs.5b02785
J. Am. Chem. Soc. 2015, 137, 6866–6879

Table 1. Molecular Weight, Polydispersity, and Percentage Regioregularity of P3HT, F-P3HT, P3OT, F-P3OT, P3EHT, and F-P3EHT

polymer	M_n (kDa)[a]	M_w (kDa)[a]	Đ	rr[b] (%)
P3HT	39	55	1.4	97
F-P3HT	–[c]	–[c]	–[c]	93
P3OT	19	26	1.4	95
F-P3OT	23	41	1.8	96
P3EHT	29	44	1.5	97
F-P3EHT	28	37	1.3	96

[a]Measured by GPC in chlorobenzene at 80 °C relative to polystyrene standards. [b]Measured by integration of the methylene region by ^{1}H NMR. [c]Molecular weight of F-P3HT could not be measured due to low solubility.

NMR spectra (Figures S5–S7, S10–12) as shown in Table 1. F-P3HT showed a relatively low rr degree of 93% likely due to the low molecular weight and resulting end-group effects, while F-P3OT and F-P3EHT exhibited high rr's greater than 96% (and comparable to those of the non-fluorinated polymers) The ^{19}F NMR spectrum (Figures S8 and S9) of F-P3OT and F-P3EHT exhibited a single resonance, providing additional evidence for the high degree of uniformity of the backbone of these polymers.

Polymer Thermal Properties. The thermal properties of the polymers were evaluated by DSC under nitrogen. The first (P3EHT) and second (P3HT, F-P3HT, P3OT, F-P3OT, and F-P3EHT) heating and cooling DSC curves are shown in Figure 1. The detailed thermal data including melting and

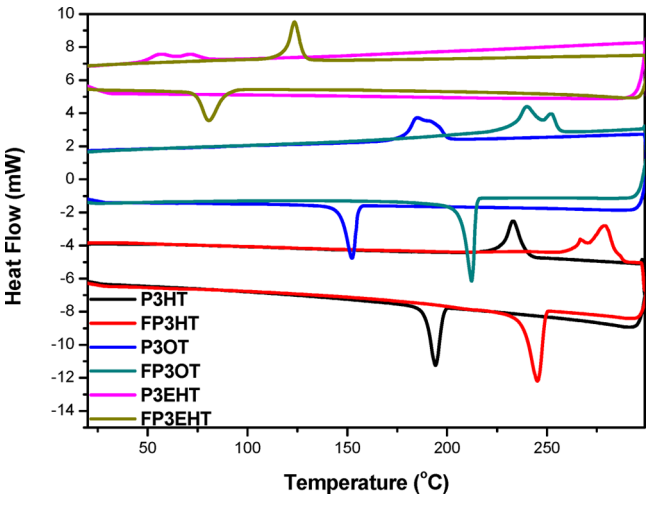

Figure 1. DSC heating and cooling traces of P3EHT (first cycle) and P3HT, F-P3HT, P3OT, F-P3OT, and F-P3EHT (second cycle) at a scanning speed of 10 °C/min under N_2 (endo up). Note: traces offset for clarity.

cooling peaks, as well as the corresponding enthalpy values are presented in Table 2. F-P3HT exhibits two endothermic peaks at 267 and 279 °C and a single exothermic peak upon cooling at 245 °C, which are higher than those of P3HT (233 and 194 °C). In addition to raising the melting point, introducing the F atom to the backbone has a clear influence on the crystallization enthalpy, with F-P3HT exhibiting significantly higher values than P3HT (ca. 32 J/g vs ca. 19 J/g). Although care needs to be taken in the interpretation of polymer enthalpy values, this significant increase suggests that attractive intermolecular interactions in the fluorinated polymer are increased compared to those in the non-fluorinated polymer. Similar to F-P3HT, F-P3OT also showed significantly higher melting temperatures and crystallization enthalpy compared to P3OT. The melting temperature and crystallization enthalpy of F-P3OT are both decreased in comparison to those of F-P3HT as a result of the increased side-chain length. Interestingly, both of the fluorinated polymers display double endotherms upon melting, which may indicate the presence of different polymorphs within the sample.

The difference in the thermal behavior of the branched EH containing polymers is perhaps most striking. As has been previously reported P3EHT exhibits two melting peaks in the initial heating cycle, but forms a glass upon relatively rapid cooling in the DSC.[32] The glass slowly crystallizes over time as a thin film, or by sustained (1 h) thermal annealing close to the melting point.[32] The slow crystallization kinetics have been related to the irregular geometry of the side chains due to the stereocenter in the EH group.[33] However, upon fluorination, the thermal behavior changed significantly, and F-P3EHT showed a clear melting and crystallization peak, with an increase in melting point of around 50 °C compared to that of P3EHT. The thermal transitions of F-P3EHT are fully reversible and reproducible in subsequent cycles, in contrast to P3EHT.

Optical and Electronic Properties. The UV–visible absorption spectra of the polymers in dilute 1,2-dichlorobenzene (DCB) and hot DCB, and as spin-coated films from DCB, are shown in Figure 2, and the data are summarized in Table 2. In dilute DCB solution at room temperature, P3HT, P3OT, P3EHT, and F-P3EHT all exhibit a single absorption peak indicative of good dissolution, whereas the fluorinated straight-chain polymers F-P3HT and F-P3OT show clear signs of aggregation, with spectra that resemble those of the solid-state films. Upon heating, the absorption maxima of P3HT, P3OT, P3EHT, and F-P3EHT all blue shift slightly, indicating there is not a strong aggregation between polymer backbones in dilute solution. F-P3HT and F-P3OT show pronounced blue-shifts (121 and 118 nm) upon heating, as the interaction between polymer backbones is reduced, presumably due to increased torsional twisting. F-P3HT still shows signs of aggregation even in hot DCB solution, with small vibronic peaks observable at 539 and 584 nm. In addition the λ_{max} of the branched polymers are more blue-shifted in hot solution than either of their straight chain analogues, suggesting the branched EH group causes more perturbation to the conjugated backbone than the straight chain thereby disrupting conjugation.

The spectral shape of all four of the straight chain polymers is very similar upon film formation, with the appearance of clearly defined vibronic shoulders to the red of the maximum absorption peak, which are indicative of intermolecular interactions.[34] For the fluorinated straight chain polymers, film formation from hot DCB was difficult to control, and spin coating from hot TCB was found to afford better reproducibility. There was little difference in the spectra of films obtained from DCB or TCB for either P3OT or F-P3OT (Figure S13). Annealing of the films up to 125 °C did not result in significant changes to the spectra, although there were some subtle changes in the relative intensity of the long wavelength shoulder peaks (Figures S14 and S15). The peaks for the fluorinated polymers are slightly blue-shifted in comparison to those for the non-fluorinated polymers, with an increased optical band gap of 1.98 eV for the fluorinated straight chain

DOI: 10.1021/jacs.5b02785
J. Am. Chem. Soc. 2015, 137, 6866–6879

Table 2. Physical Properties of P3HT, F-P3HT, P3OT, F-P3OT, P3EHT, and F-P3EHT

				UV−vis (nm)				
polymer	T_m[a] (°C)	T_c[a] (°C)	$\Delta H(T_c)$ (J/g)	RT DCB	hot DCB	film	E_g, opt[c] (eV)	IP[d] (eV)
P3HT	233	194	19	457	452	524, 558, 602	1.91	−4.64
F-P3HT	267, 279	245	32	507, 540, 584	419, 539, 584	509, 538, 584	1.98	−5.10
P3OT	184, 191	152	17	455	449	527, 559, 604	1.91	−4.70
F-P3OT	240, 252	212	28	431, 507, 538, 583	416	511, 539, 586	1.98	−4.99
P3EHT	56, 72[b]	–	–	443	432	490, 526, 567	2.03	−4.95
F-P3EHT	123	81	20	416	410	503, 539, 584	1.98	−5.20

[a]Melting temperature (T_m) and crystallization temperature (T_c) determined by DSC. [b]Data from first cycle of DSC trace. [c]Optical band gap estimated from the low-energy band edge in the optical spectrum. [d]Ionization potential level in thin film measured from PESA data (error ±0.05 eV).

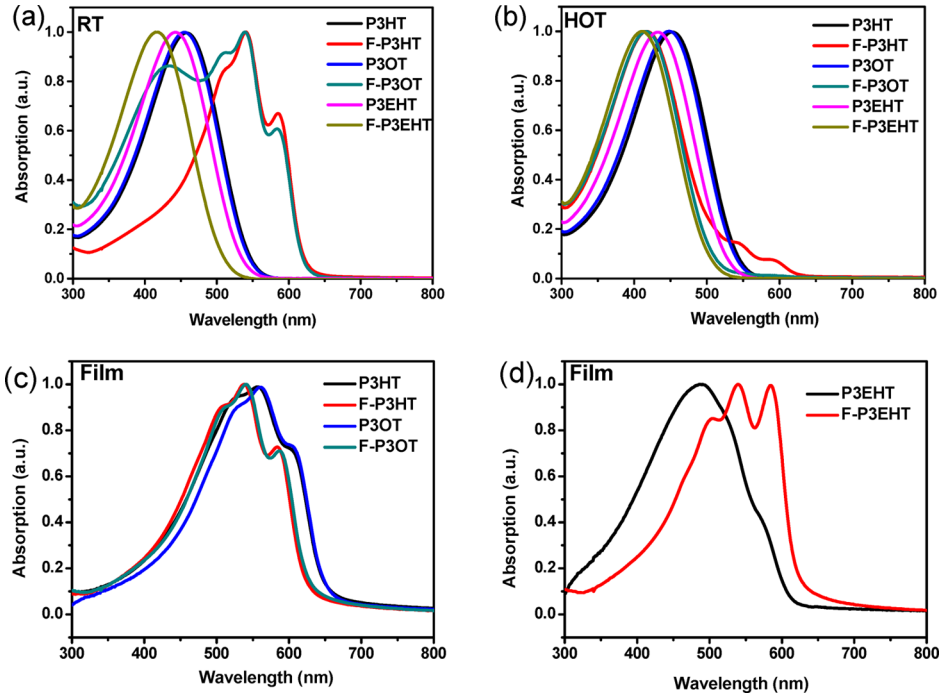

Figure 2. UV−vis absorption spectra of P3HT, F-P3HT, P3OT, F-P3OT, P3EHT, and F-P3EHT (a) in dilute dichlorobenzene solution at room temperature and (b) in dichlorobenzene solution at 90 °C, (c) of as-spun films of P3HT, F-P3HT, P3OT, and F-P3OT, and (d) of as-spun films of P3EHT and F-P3EHT.

derivatives in comparison to 1.91 eV for the non-fluorinated. Again substantial differences are observed in the case of the branched EH polymers. The spectrum of the as-cast P3EHT is very similar to that reported previously,[33,35] with a maximum around 490 nm and two weak shoulders at higher wavelengths. The band gap is also substantially wider than the straight chain derivatives, at 2.03 eV, suggesting that conjugation is disrupted in the solid state, most likely as a result of the increased size and mixed stereoisomers of the side chain. In contrast, the as-cast F-P3EHT spectrum is substantially different and displays a sharp and strong vibronic shoulder of almost equal intensity to the main absorption band. The red-shift between solution and solid λ_{max} at 123 nm is also substantially increased compared to the 47 nm observed for the non-fluorinated polymer, suggesting that the fluorinated polymer is better able to planarize in the solid state. The intensity of this vibronic shoulder versus the main absorption peak has been related to the degree of intermolecular ordering and aggregation in the thin film for P3HT, according to the weakly interacting H-aggregation model of Spano and co-workers.[36] Although this may not be directly applicable for the branched-side-chain polymer, the strong vibronic peaks certainly suggests pronounced coupling between the optical dipoles in the solid state and along with the pronounced red-shift, suggesting that backbone fluorination partly overcomes the propensity of the branched EH group to perturb backbone planarity.

The energetics of the polymers in thin films were investigated by a combination of PESA and UPS measurements in ultra-high vacuum. The PESA measurements show a consistent increase in ionization potential upon backbone fluorination of around 0.3 eV, which we ascribe primarily due to the strong electron-withdrawing influence of the F atom. The effect of increasing side-chain length or branching on both of the P3AT series is to increase ionization potential of the film. In the case of F-P3HT, we believe the low molecular weight and reduced rr may give an anomalously high ionization potential. The branching of the side chain clearly causes an increase in ionization potential for both the fluorinated and the non-fluorinated analogues, although the magnitude is smaller for the fluorinated polymer, in agreement with the idea that the branched EH side chain increases backbone perturbation.

DOI: 10.1021/jacs.5b02785
J. Am. Chem. Soc. 2015, 137, 6866−6879

In order to further investigate the energetics of the polymers with and without fluorination, UPS studies were performed on the P3OT and F-P3OT, with the spectra shown in Figure 3 and

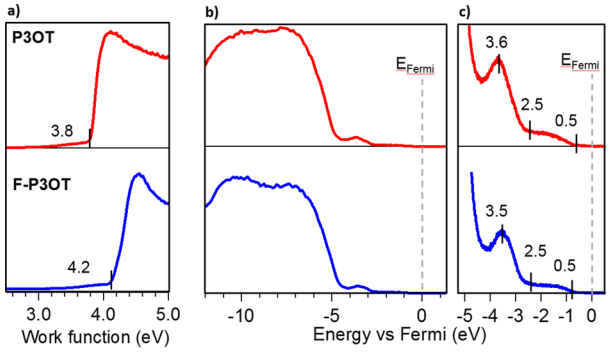

Figure 3. Ultraviolet photoemission spectroscopy of spin-coated films of P3OT and F-P3OT.

the energy band diagrams in Figure S16. In Figure 3a the UPS spectra show the onset of the secondary edge, which is used to determine the work function of the materials, as defined by the energy difference between the Fermi level and the local surface vacuum level. In Figure 3b,c the observed spectra are representative of the local density of states associated with the two polymer films, with the corresponding energies reported with respect to the Fermi level. In Figure 3c, three relevant energies have been identified: i.) the low-energy onset of the easiest ionized, highest occupied states (~0.5 eV below the Fermi) associated with tailing intragap states and typically used to define the polymer ionization potential; ii.) the onset of the main HOMO-like feature (~2.5 eV below Fermi), attributed to the sp^2-hybridized orbitals; and iii.) the local maximum of the HOMO-like feature (~3.5−3.6 eV below the Fermi). We detect two observable differences upon fluorination of the thiophene backbone. The first is the increase in the polymer work function, from 3.8 to 4.2 eV (Figure 3a). In Figure 3b, there is a change in the density of states for the two peak-like features, one at ~10 eV and the other at ~7 eV below the Fermi level; both of these regions are consistent with fluorination (F 2p atomic orbitals). However, there is very little observed difference in the valence band feature shape or energies with respect to the Fermi level (Figure 3c), which is suggestive of minimal change to the HOMO-like features of the polymers. This is not surprising, given that the HOMO of P3HT is well-known to be highly delocalized. When combining the differences in the work function with the observed valence features into a band diagram (Figure S16), we readily observe that the major change in the ionization potential is due to the change in the surface vacuum level, as manifested in the reported change in the work function. However, it is important to note that there were some subtle changes in the core levels, as observed by XPS, which are given in the Supporting Information (Figure S17).

Computational Studies. To help explain the influence of fluorination on both the polymer energy levels and the physical structure, DFT calculations of hexamers of P3AT and F-P3AT were modeled using Gaussian at the B3LYP/6-31G* level. The side chains were modified to methyl groups in order to simplify the calculations. For each hexamer an all trans configuration with respect to adjacent thiophenes was allowed to relax to its energy minima. Frequency calculations were performed on the lowest energy conformations to ensure the geometry was not the result of a local minima. The minimum-energy conformations of both hexamers are shown in Figure 4.

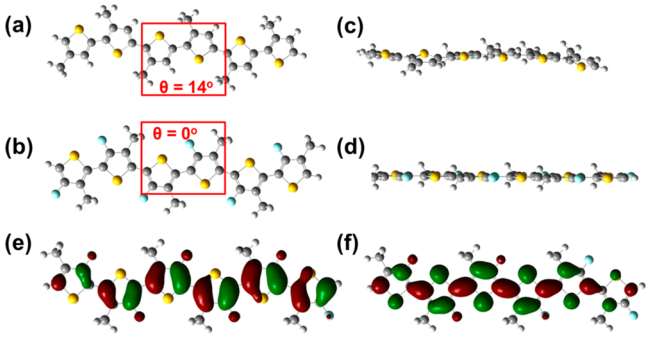

Figure 4. Top view of energy-minimized structures of a methyl-substituted hexameric (a) P3AT and (b) F-P3AT. Side view of energy-minimized structure of (c) a methyl-substituted P3AT and (d) F-P3AT. HOMO (e) and LUMO (f) distributions for the energy-minimized structure of F-P3AT. All calculated using DFT at the B3LYP/6.31G(d,p) level.

Consistent with other reports,[37] the calculations clearly show that P3AT has a slightly twisted backbone conformation, with a torsion angle (θ) of 14° between the central two thiophene rings and slightly larger twist angles toward the terminal thiophene rings. In contrast F-P3AT possesses a completely planar backbone conformation, with all thiophene rings co-planar to one another. Upon closer inspection of the Mülliken partial charges on the atoms in the model, we believe the origin of this planarization could be electrostatic in nature, as the positively charged sulfur atom (+0.308) and negatively charged fluorine atom (−0.281) are in close proximity in F-P3AT. In P3AT on the other hand, while the sulfur is still positively charged (+0.264), the hydrogen is also positively charged (+0.148), causing a slightly repulsive interaction and hence a backbone twist.

To further investigate the conformational preference of the fluorinated and non-fluorinated rings, we performed relaxed potential energy scans (PES) for two model hexamers of head-to-tail 3-methylthiophene, both fluorinated and non-fluorinated. We chose hexamers since they have been shown to be much more representative of a polymer chain than a simple dimer.[37] Here the inter-ring C−C bond between the central two thiophenes was fixed at a set angle (θ), and all other degrees of freedom were allowed to relax to their potential energy minima at a hybrid DFT B3LYP/6-31G* level of calculation. The total energy for each conformer as a function of interring bond angle is shown in Figure 5a, where 0° corresponds to the cisoid configuration and ±180° to the transoid configuration. The PES profile for the non-fluorinated hexamer is very similar to that previously reported by DFT for a fully hexyl-substituted hexamer,[37] and shows two energy minima at a dihedral angles of ±170° and ±30° from the cisoid co-planar configuration. The profile exhibits global maxima at ±90° when the thiophenes are fully twisted out of conjugation, as well as a local maxima at 0° and ±180° for the fully co-planar cis or transoid conformations. The cisoid conformation is higher in energy than the transoid due to steric interaction between the methyl group and the 3-hydrogen of the thiophene ring. Upon moving to the fluorinated hexamer, we now find that the energy minima are at ±180°, i.e. fully co-

DOI: 10.1021/jacs.5b02785
J. Am. Chem. Soc. 2015, 137, 6866−6879

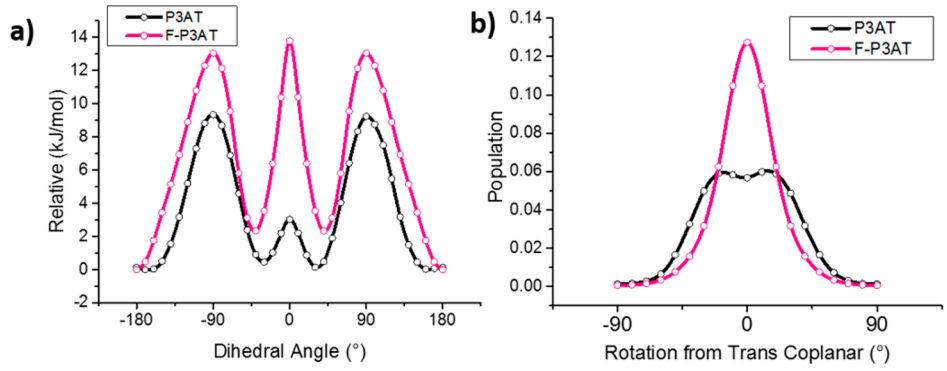

Figure 5. a) Potential energy distribution of P3AT and F-P3AT, where A = methyl. A dihedral angle of 0° corresponds to the cisoid conformation; b) Relative probability densities for populating the energy distribution with a Boltzmann energy distribution at room temperature. A dihedral angel of 0° corresponds to the transoid configuration.

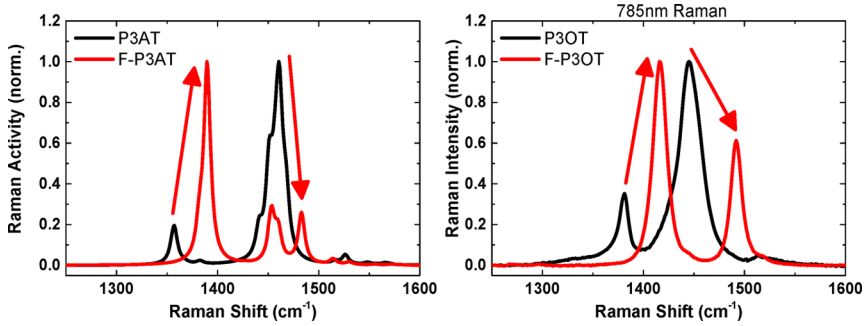

Figure 6. (a) DFT-calculated Raman spectra of P3AT and F-P3AT, where A = methyl. (b) Experimental Raman spectra at room temperature of P3OT and F-P3OT.

planar in the transoid conformation, and at ±40°. These results are in agreement with calculations upon 3,4-difluorothiophene dimers, which also predict a fully co-planar transoid conformation.[38] The profile now exhibits three maxima, at ±90° identical to the non-fluorinated hexamer as the rings twist fully out of conjugation. Significantly, however, the fully co-planar cisoid conformation (0°) now becomes a high-energy conformation due the steric interaction between the methyl group and the fluorine substituent. The energy barrier to rotate through this conformation becomes significantly larger for the case of the fluorinated hexamer versus the non-fluorinated (ca. 10 kJ/mol).

Another important difference is that fluorination significantly steepens the potential energy surface in the regions around the energy minima. This is shown in the transoid region in Figure 5b, where the degrees of freedom are populated with a Boltzmann distribution at room temperature. This suggests that the polymer backbone is significantly more co-planar and stiffer upon fluorination.

Taken together, these data suggest, therefore, that fluorination of the thiophene backbone will lead to an increase in co-planarity of the polymer backbone for sections where the polymer is able to adopt an all trans configuration leading to a more rigid backbone. A more rigid backbone would be in agreement with the higher tendency to aggregate observed experimentally, as well as the increased melting temperatures. However, when the fluorinated polymer does adopt the cisoid configuration of adjacent thiophenes, the barrier to reorganization by rotation of the backbone is significantly larger, which may hinder solid-state reorganization and crystallization. In addition, the higher energy of the fully co-planar cisoid conformation may prevent full planarization even in the solid state when solid-state packing forces are known to promote planarization of the thiophene oligomers.

Similar to P3AT (Figure S18), the HOMOs and LUMOs of F-P3AT were predicted to be delocalized over the entire conjugated backbones (Figure 4e,f). The HOMO is predominantly aromatic, and the LUMO is mainly of quinoidal character. The difference between P3AT and F-P3AT is that the F atom contributes to both HOMO and LUMO, which means that the F atom can affect both the HOMO and LUMO levels. The calculated HOMO and LUMO of P3AT and F-P3AT are −4.64 and −2.16 eV, and −4.78 and −2.40 eV, respectively, which are in good agreement with the experimentally observed trends by PESA and UPS.

Raman Investigations. The Raman spectra of polythiophene and related analogues have been extensively studied and provide useful insight into the solid-state ordering of the polymer.[39] Figure 6 compares the simulated and measured Raman spectra for P3OT and F-P3OT. The main Raman peaks lie in the range 1300−1550 cm^{-1}, which corresponds with carbon bond stretching modes in conjugated structures. The spectra of P3OT is very similar to that observed for P3HT, and so the two strong peaks measured for P3OT are readily identified as the collective backbone stretching modes of the C−C (1381 cm^{-1}) and C═C (1445 cm^{-1}) bonds. The peak positions, relative intensities, and shapes of these modes are strongly associated with the molecular conformation (primarily co-planarity) of the conjugated polymer backbone.[39]

The fluorinated polymer also has two strong Raman peaks centered at 1417 and 1492 cm^{-1}. The natures of these vibrational modes are ascertained by comparison with the DFT

DOI: 10.1021/jacs.5b02785
J. Am. Chem. Soc. 2015, 137, 6866−6879

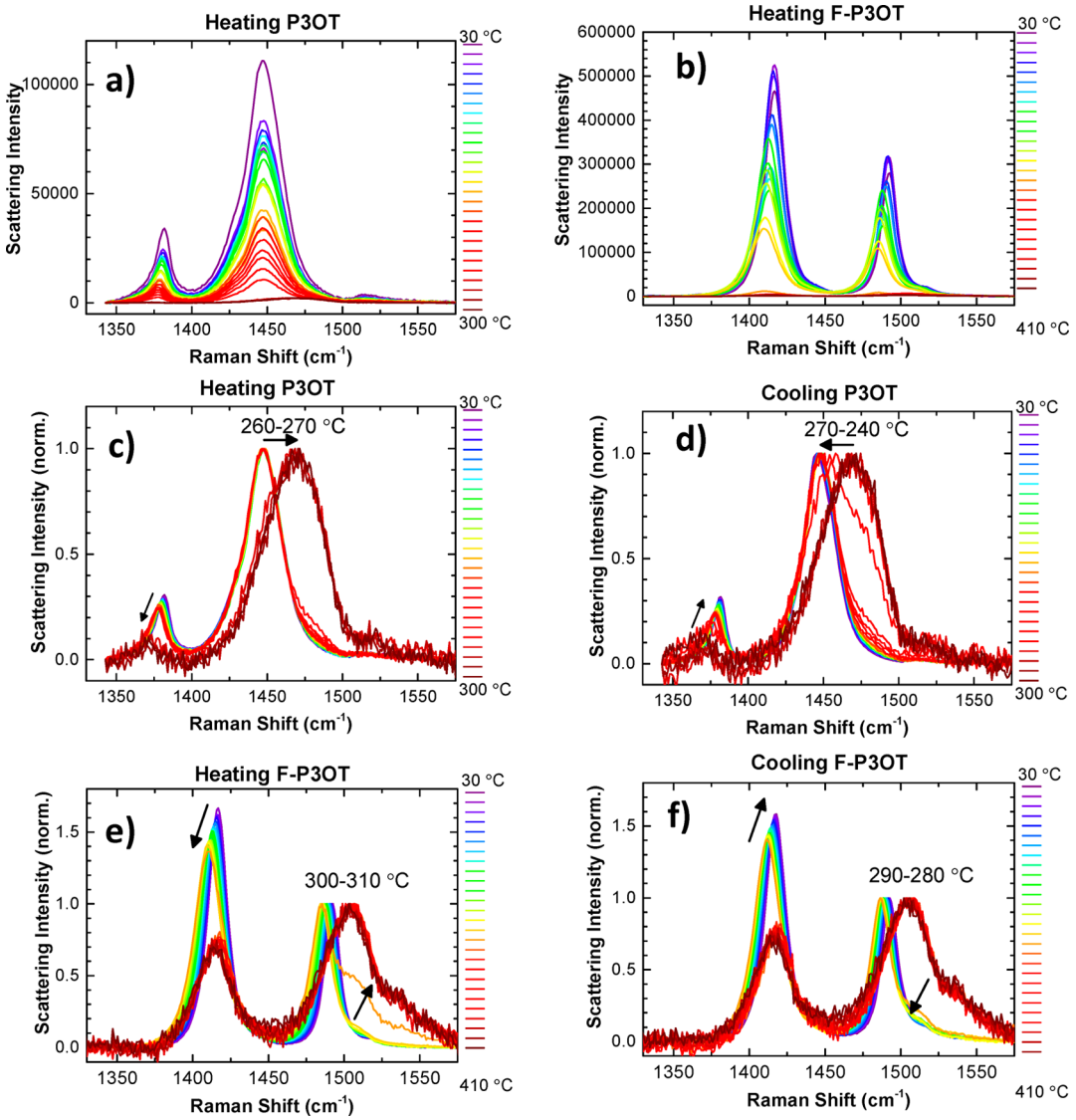

Figure 7. Raman spectra measured during heating from (a) 30 to 300 °C for P3OT and (b) 30 to 410 °C for F−P3OT. Normalized Raman spectra for P3OT during (c) heating and (d) cooling. Normalized Raman spectra for F−P3OT during (e) heating and (f) cooling.

calculations, which show similar values. The calculated P3AT has two peaks centered at 1357 and 1461 cm^{-1}, where the latter is stronger and also shows sub-peaks on the lower frequency side, leading to a skewed peak shape—these characteristics match well with the measured spectrum for P3OT. The calculated spectrum for F-P3AT has a strong peak at 1389 cm^{-1} and two weaker peaks at 1454 and 1483 cm^{-1}, where the 1454 cm^{-1} mode corresponds most closely with the shoulders on the main mode observed for the P3AT spectrum, and the 1483 cm^{-1} mode is the main C═C collective stretch shifted to higher frequency. The 1454 cm^{-1} mode in the DFT spectrum for F-P3AT is not represented in the experimental Raman spectrum, which may be attributed to the fact that the calculated Raman activity does not correspond directly to experimentally measured Raman intensities. The modes calculated at 1357 and 1389 cm^{-1} for P3AT and F-P3AT, respectively, both correspond to a collective C−C bond stretch. The effect of fluorination on the polythiophene Raman modes can be summarized as a shift in both the C−C and C═C collective stretching modes to higher frequencies, and an increase in the intensity of the C−C mode relative to the C═C mode. These effects are visible in both the simulated and experimental spectra.

In previous studies an increase in the intensity of the C−C mode relative to the C═C mode has been associated with an increased π electron density in the C−C bond resulted from the increased co-planarity of the conjugated polymer backbone,[39] providing further evidence that fluorination enhances backbone planarity. The shift of the C−C mode to higher frequency has also been associated with an increase in effective conjugation length, but this is typically accompanied by a shift of the C═C mode to lower frequency. In this case the shift of the C═C mode from 1445 to 1492 cm^{-1} upon fluorination suggests that the fluorine substitution results in an increase in force constant for the C═C bonds. This is consistent with other theoretical studies showing that fluorination leads to reduced lengths of the C−C and C═C bonds.[40] In addition to this, the narrowing in FWHM of the C═C mode peak from 26.0 cm^{-1} in P3OT to 13.1 cm^{-1} in F-P3OT suggests that the fluorinated polymer sample contains much narrower distribution of molecular conformations, which is similarly consistent

DOI: 10.1021/jacs.5b02785
J. Am. Chem. Soc. 2015, 137, 6866−6879

with the fluorinated polymer having a highly planar and rigid polymer backbone.

Temperature-Dependent Raman Spectroscopy. Figure 7 shows the changes in the Raman spectra of P3OT and F-P3OT films during heating from 30 to 300 °C (P3OT) or 410 °C (F-P3OT) under nitrogen. In both cases we observe an overall reduction in the Raman scattering intensity and shifts in the peak positions, this effect is significantly more pronounced for P3OT than F-P3OT.

A clearer comparison is achieved by normalizing the spectra. Figure 7c,d shows the normalized spectra for both heating and cooling for P3OT. In this case we find a gradual reduction in the relative intensity of the C−C mode and a shift to lower frequency at high temperatures, which is consistent with reduced molecular planarity at elevated temperature as a result of thermally induced backbone twisting, similar to that observed in other thiophene-based polymers.[41] In addition, we observe a pronounced shift in the position of the C═C peak from 1445 to 1469 cm^{-1} occurring between 260 and 270 °C, which reverses more gradually upon cooling (270−240 °C). This transition is indicative of a significant conformational change and may represent the temperature at which the energetic rotational barrier for the inter-thiophene bond is fully overcome to allow full rotational freedom of the backbone. We note the transition occurs at a higher temperature than the melt transitions identified using DSC. The Raman spectrum of F-P3OT shows a similar temperature dependence, as shown by the normalized spectra in Figure 7e,f. In this case the C−C mode again shifts to lower energy at high temperatures and decreases in relative intensity, though now the C═C peak shifts toward lower energy (1492 to 1485 cm^{-1}) at temperatures up to 300 °C before a sudden loss of intensity and a shift to around 1505 cm^{-1} between 300 and 310 °C. This sharp transition reverses more gradually upon cooling at 290−280 °C. This transition at 300−310 °C for F-P3OT shows the same characteristics as that observed at 260−270 °C for P3OT, and the increase in transition temperature for F-P3OT supports the suggestion that the fluorinated polythiophene has a more planar and rigid backbone with a greater inter-unit rotational barrier.

Thin-Film Morphology. Figure 8 shows the 2D GIWAXS patterns of the fluorinated and non-fluorinated P3OT and P3EHT films prepared by spin-coating. P3OT shows a series of alkyl stacking reflections along q_z corresponding to edge-on oriented crystallites. F-P3OT also shows a series of alkyl stacking reflections along q_z however these peaks are broader with an increased orientational distribution. The alkyl stacking distance is determined to be 19.57 Å for P3OT with a slightly smaller value of 19.07 Å for F-P3OT (see Table 3). Scherrer analysis of the first alkyl stacking peak yields a coherence length of 12.9 nm for P3OT, which is larger than that of F-P3OT (9.8 nm). Taken together, these observations indicate that fluorination of P3OT frustrates crystallization with reduced crystalline order, at least along the alkyl stacking direction. The 2D GIWAXS pattern of P3EHT, Figure 8c, is consistent with previous observations with additional mixed-index peaks in addition to the alkyl stacking peaks that are observed along q_z.[33] The scattering pattern of P3EHT has been indexed to a triclinic unit cell rather than an orthorhombic cell typically observed for poly(3-alkythiophenes).[33] Similar to the case for P3OT, fluorination of F-P3EHT leads to reduced crystalline order with only weak scattering observed. The alkyl stacking distance for F-P3EHT of 13.67 Å is similarly reduced compared to that of P3EHT (14.33 Å). A dramatic decrease in the alkyl stacking

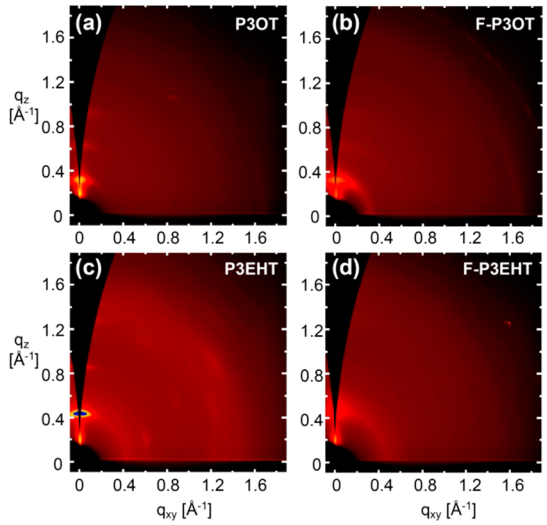

Figure 8. Two-dimensional GIWAXS images of spun-cast films of (a) P3OT, (b) F-P3OT, (c), P3EHT, and (d) F-P3EHT. Films were prepared from hot 1,2,4-trichlorobenzene (a,b) or hot chloroform (c,d).

Table 3. Summary of GIWAXS Peak Fitting Results

	alkyl-stacking		π-stacking	
polymer	d-spacing (Å)	coherence length (Å)	d-spacing (Å)	coherence length (Å)
P3OT	19.57 ± 0.01	129 ± 2	3.88 ± 0.002	68 ± 1
F-P3OT	19.07 ± 0.02	98 ± 2	3.91 ± 0.002	55 ± 2
P3EHT	14.33 ± 0.01	188 ± 2	3.54 ± 0.002	28 ± 3
F-P3EHT	13.67 ± 0.02	67 ± 2	3.82 ± 0.002	87 ± 28

coherence length is also seen dropping from 18.8 nm for P3EHT to 6.7 nm for F-P3EHT. Weak π-stacking peaks are also observed in plane (along q_{xy}) with π-stacking distances of 3.88 Å for P3OT and a slightly larger value of 3.91 Å for F-P3OT. Coherence lengths of 6.8 nm are found for P3OT along the π-stacking direction compared to 5.5 nm for F-P3OT. π-stacking peaks are also observed for P3EHT and F-P3EHT, although these are likely to be associated with the liquid crystalline (rather than crystalline) component of the film. Nevertheless, a π-stacking distance and corresponding coherence length of 3.54 Å and 2.8 nm respectively are observed for P3EHT, and 3.82 Å and 8.7 nm respectively for F-P3EHT.

The suppressed degree of thin-film crystalline order evident upon fluorination could be the result of the reduced rotational freedom of the fluorinated polythiophene backbone discussed earlier. Thus, while the enhanced planarity of the all-trans sections of fluorinated polymer might be expected to lead to the signs of aggregation and short-range order apparent by thermal and spectroscopic techniques, the higher rotational barrier of the fluorinated polymers in a cis arrangement may lead to "trapping" of the polymer is this conformation and therefore reduced long-range order.

Charge Transport Behavior in Field Effect Transistors. The charge carrier transport behavior was investigated in FETs in a bottom contact, top gate configuration using gold source−drain electrodes. Due to the poor solubility of the straight chain fluorinated polymers, films were formed in all cases by zone-casting from hot 1,2-dichlorobenzene under identical conditions. The zone-casting technique gives excellent control over the film formation, since both solvent temperature and

DOI: 10.1021/jacs.5b02785
J. Am. Chem. Soc. 2015, 137, 6866−6879

substrate temperature can be readily controlled.[42] Following the semiconductor film deposition, the dielectric (PMMA) was deposited by spin coating, followed by thermal evaporation of the gate electrode. In the case of the P3EHT, the high solubility of the polymer in the solvent used to deposit PMMA (*n*-butylacetate) necessitated the use of a fluorinated dielectric, Cytop, which could be deposited from a non-solvent for the polymer. To allow for a consistent comparison, Cytop was utilized for both P3EHT and F-P3EHT. The results of the transistor measurements are summarized in Table 4, and the individual transfer and output plots are shown in Figure 9 and Figures S19–S22.

Table 4. Summary of Average and Peak FET Mobility (Channel Length and Channel Width 20 μm and 1 mm, Respectively)

	μ_{lin} (cm^2 V^{-1} s^{-1})		μ_{sat} (cm^2 V^{-1} s^{-1})	
material	average	maximum	average	maximum
P3HT	0.088	0.13	0.16	0.49
F-P3HT	0.14	0.26	0.22	0.47
P3OT	0.14	0.18	0.13	0.18
F-P3OT	0.70	0.81	0.44	0.53
P3EHT[a]	4.35×10^{-4}	1.48×10^{-3}	6.91×10^{-4}	1.84×10^{-3}
F-P3EHT[a]	2.46×10^{-3}	6.45×10^{-3}	3.09×10^{-3}	6.66×10^{-3}

[a]Cytop was used as gate dielectric; all other examples utilized PMMA.

All transistors exhibited p-type behavior with negligible operating hysteresis, good drain current saturation, and on/off current ratios in the range of 10^4–10^5. From the transistor measurements it is clear that fluorination generally results in a significant increase in average charge carrier mobility for both the linear and saturated mobility. This is most pronounced in the comparison of the F-P3OT and F-P3EHT with their non-fluorinated counterparts. In the case of the hexyl-substituted polymers, the difference is more modest, which may be related to differences in the molecular weight of the fluorinated and non-fluorinated polymers. It is interesting that despite the reduced crystalline order upon fluorination evident from the GIWAXS data, fluorination clearly has a positive effect on charge carrier mobility. The increased mobility is in agreement with the evidence suggesting a more planar backbone arrangement for the fluorinated materials, as a higher degree of planarity can improve both intra- and intermolecular charge transport. These results further confirm recent studies suggesting that backbone rigidity and co-planarity are important design features for high-performance transistor materials.[43]

CONCLUSIONS

We have reported two strategies toward the synthesis of the useful building block 2,5-dibromo-3-alkyl-4-fluorothiophene. The presence of the fluorine substituent on the thiophene was shown to have a pronounced directing effect on the Grignard metathesis reaction, leading to almost quantitative formation of 2-bromo-3-alkyl-4-fluoro-5-thienyl magnesium bromide, as opposed to a roughly 4:1 mixture of the 2-bromo and 5-bromo isomers in the absence of the fluorine group. Polymerization of the Grignard monomer by the addition of a Ni(II)dpppCl$_2$ catalyst afforded highly regioregular polymers of good molecular weight.

Comparison of the fluorinated polymers with their analogous non-fluorinated counterparts demonstrates that fluorination results in a considerable increase in polymer ionization potential. The fluorinated and non-fluorinated polymers exhibited very similar optical band gaps, indicating that fluorination leads to a lowering of both the HOMO and LUMO energy levels. Significant differences were observed in the physical behavior of the polymers, with fluorination leading to a reduction in polymer solubility, as well as substantial increases in melting temperature and crystallization enthalpy. These changes are consistent with a more planar, rigid polymer

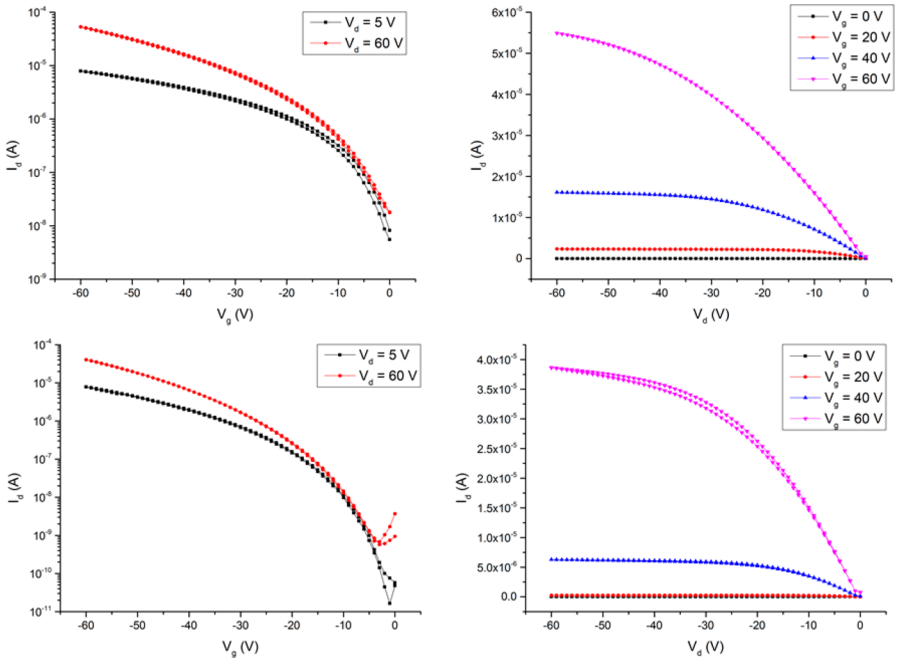

Figure 9. P3HT (top) and F-P3HT (bottom) transfer and output characteristics (channel length and width of 20 μm and 1 mm, respectively; PMMA dielectric).

DOI: 10.1021/jacs.5b02785
J. Am. Chem. Soc. 2015, 137, 6866–6879

backbone, which leads to enhanced aggregation in the solid state. However, this enhanced aggregation does not lead to any increase in thin-film crystalline order compared to that of the non-fluorinated polymer, likely as a result of reduced rotational freedom upon fluorination. Fluorination also results in a significant increase in charge carrier mobility in transistor devices, with average mobilities increasing 5-fold upon fluorination to values around 0.7 $cm^2/(V\ s)$. We believe these results demonstrate that backbone fluorination of polythiophene and its analogues is a useful strategy to optimize the solid-state packing and performance in a range of optoelectronic devices.

■ ASSOCIATED CONTENT

Supporting Information

Additional figures as mentioned in the text, including GCMS, monomer and polymer NMR, DFT calculations, UV−vis spectra of annealed films, and FET plots. The Supporting Information is available free of charge on the ACS Publications website at DOI: 10.1021/jacs.5b02785.

■ AUTHOR INFORMATION

Corresponding Author

*m.heeney@imperial.ac.uk

Notes

The authors declare no competing financial interest.

■ ACKNOWLEDGMENTS

This work was supported by EPSRC grants EP/G060738/1 and EP/K029843/1, a KAUST Competitive Research grant under agreement no. CRG-1-2012-THO-015, and the Australian Research Council (FT100100275, DP130102616). We thank Dr. Scott E. Watkins (CSIRO Melbourne) for the PESA measurements. Part of this research was undertaken on the SAXS/WAXS beamline at the Australian Synchrotron, Victoria, Australia.

■ REFERENCES

(1) (a) Mishra, A.; Ma, C. Q.; Bauerle, P. *Chem. Rev.* **2009**, *109*, 1141. (b) Osaka, I.; McCullough, R. D. *Acc. Chem. Res.* **2008**, *41*, 1202. (c) Zhang, L.; Colella, N. S.; Cherniawski, B. P.; Mannsfeld, S. C. B.; Briseno, A. L. *ACS Appl. Mater. Interfaces* **2014**, *6*, 5327.

(2) Nielsen, C. B.; McCulloch, I. *Prog. Polym. Sci.* **2013**, *38*, 2053.

(3) Dang, M. T.; Hirsch, L.; Wantz, G. *Adv. Mater.* **2011**, *23*, 3597.

(4) McCullough, R. *Adv. Mater.* **1998**, *10*, 93.

(5) Okamoto, K.; Luscombe, C. K. *Polym. Chem.* **2011**, *2*, 2424.

(6) Bannock, J. H.; Krishnadasan, S. H.; Nightingale, A. M.; Yau, C. P.; Khaw, K.; Burkitt, D.; Halls, J. J. M.; Heeney, M.; de Mello, J. C. *Adv. Funct. Mater.* **2013**, *23*, 2123.

(7) Liu, J.; McCullough, R. D. *Macromolecules* **2002**, *35*, 9882.

(8) (a) Sheina, E. E.; Liu, J.; Iovu, M. C.; Laird, D. W.; McCullough, R. D. *Macromolecules* **2004**, *37*, 3526. (b) Yokoyama, A.; Miyakoshi, R.; Yokozawa, T. *Macromolecules* **2004**, *37*, 1169.

(9) (a) Bhatt, M. P.; Magurudeniya, H. D.; Rainbolt, E. A.; Huang, P.; Dissanayake, D. S.; Biewer, M. C.; Stefan, M. C. *J. Nanosci. Nanotechnol.* **2014**, *14*, 1033. (b) Bryan, Z. J.; McNeil, A. J. *Macromolecules* **2013**, *46*, 8395.

(10) (a) McCulloch, I.; Bailey, C.; Giles, M.; Heeney, M.; Love, I.; Shkunov, M.; Sparrowe, D.; Tierney, S. *Chem. Mater.* **2005**, *17*, 1381. (b) Abdou, M. S. A.; Orfino, F. P.; Son, Y.; Holdcroft, S. *J. Am. Chem. Soc.* **1997**, *119*, 4518.

(11) Marrocchi, A.; Lanari, D.; Facchetti, A.; Vaccaro, L. *Energy Environ. Sci.* **2012**, *5*, 8457.

(12) Guo, X.; Baumgarten, M.; Müllen, K. *Prog. Polym. Sci.* **2013**, *38*, 1832.

(13) Politis, J. K.; Nemes, J. C. *J. Am. Chem. Soc.* **2001**, *123*, 2537.

(14) Heeney, M.; Zhang, W.; Crouch, D. J.; Chabinyc, M. L.; Gordeyev, S.; Hamilton, R.; Higgins, S. J.; McCulloch, I.; Skabara, P. J.; Sparrowe, D.; Tierney, S. *Chem. Commun.* **2007**, 5061.

(15) Jahnke, A. A.; Djukic, B.; McCormick, T. M.; Buchaca Domingo, E.; Hellmann, C.; Lee, Y.; Seferos, D. S. *J. Am. Chem. Soc.* **2013**, *135*, 951.

(16) (a) Li, Y.; Vamvounis, G.; Holdcroft, S. *Macromolecules* **2002**, *35*, 6900. (b) Koo, B.; Sletten, E. M.; Swager, T. M. *Macromolecules* **2015**, *48*, 229.

(17) (a) Li, L.; Counts, K. E.; Kurosawa, S.; Teja, A. S.; Collard, D. M. *Adv. Mater.* **2004**, *16*, 180. (b) Li, L.; Collard, D. M. *Macromolecules* **2005**, *38*, 372. (c) Robitaille, L.; Leclerc, M. *Macromolecules* **1994**, *27*, 1847. (d) Hong, X. Y.; Tyson, J. C.; Middlecoff, J. S.; Collard, D. M. *Macromolecules* **1999**, *32*, 4232.

(18) (a) Babudri, F.; Farinola, G. M.; Naso, F.; Ragni, R. *Chem. Commun.* **2007**, 1003. (b) Losurdo, M.; Giangregorio, M. M.; Capezzuto, P.; Cardone, A.; Martinelli, C.; Farinola, G. M.; Babudri, F.; Naso, F.; Buechel, M.; Bruno, G. *Adv. Mater.* **2009**, *21*, 1115.

(19) (a) Kim, B.-G.; Jeong, E. J.; Chung, J. W.; Seo, S.; Koo, B.; Kim, J. *Nat. Mater.* **2013**, *12*, 659. (b) Gundlach, D. J.; Royer, J. E.; Park, S. K.; Subramanian, S.; Jurchescu, O. D.; Hamadani, B. H.; Moad, A. J.; Kline, R. J.; Teague, L. C.; Kirillov, O.; Richter, C. A.; Kushmerick, J. G.; Richter, L. J.; Parkin, S. R.; Jackson, T. N.; Anthony, J. E. *Nat. Mater.* **2008**, *7*, 216. (c) Crouch, D. J.; Skabara, P. J.; Lohr, J. E.; McDouall, J. J. W.; Heeney, M.; McCulloch, I.; Sparrowe, D.; Shkunov, M.; Coles, S. J.; Horton, P. N.; Hursthouse, M. B. *Chem. Mater.* **2005**, *17*, 6567. (d) Subramanian, S.; Park, S. K.; Parkin, S. R.; Podzorov, V.; Jackson, T. N.; Anthony, J. E. *J. Am. Chem. Soc.* **2008**, *130*, 2706.

(20) Serdyuk, O.; Abaev, V.; Butin, A.; Nenajdenko, V. In *Fluorine in Heterocyclic Chemistry, Vol. 1*; Nenajdenko, V., Ed.; Springer International Publishing: Berlin, 2014; p 233.

(21) (a) Sakamoto, Y.; Komatsu, S.; Suzuki, T. *J. Am. Chem. Soc.* **2001**, *123*, 4643. (b) Osuna, R. M.; Ortiz, R. P.; Ruiz Delgado, M. C.; Sakamoto, Y.; Suzuki, T.; Hernández, V.; López Navarrete, J. T. *J. Phys. Chem. B* **2005**, *109*, 20737.

(22) El Kassmi, A.; Fache, F.; Lemaire, M. *J. Electroanal. Chem.* **1994**, *373*, 241.

(23) Gohier, F.; Frère, P.; Roncali, J. *J. Org. Chem.* **2013**, *78*, 1497.

(24) (a) Crouch, D. J.; Sparrowe, D.; Heeney, M.; McCulloch, I.; Skabara, P. J. *Macromol. Chem. Phys.* **2010**, *211*, 2642. (b) Huang, L.; Yang, D.; Gao, Q.; Liu, Y.; Lu, S.; Zhang, J.; Li, C. *Chin. J. Chem.* **2013**, *31*, 1385. (c) Fei, Z. P.; Shahid, M.; Yaacobi-Gross, N.; Rossbauer, S.; Zhong, H. L.; Watkins, S. E.; Anthopoulos, T. D.; Heeney, M. *Chem. Commun.* **2012**, *48*, 11130. (d) Jo, J. W.; Jung, J. W.; Wang, H.-W.; Kim, P.; Russell, T. P.; Jo, W. H. *Chem. Mater.* **2014**, *26*, 4214.

(25) Heeney, M.; Farrand, L.; Giles, M.; Thompson, M.; Tierney, S.; Shkunov, M.; Sparrowe, D.; McCulloch, I. U.S. Patent 6676857 B2, 2004.

(26) Kirby, N. M.; Mudie, S. T.; Hawley, A. M.; Cookson, D. J.; Mertens, H. D. T.; Cowieson, N.; Samardzic-Boban, V. *J. Appl. Crystallogr.* **2013**, *46*, 1670.

(27) (a) Becke, A. D. *J. Chem. Phys.* **1993**, *98*, 5648. (b) Frisch, M. J.; Trucks, G.; Schlegel, H. B.; Scuseria, G.; Robb, M.; Cheeseman, J.; Scalmani, G.; Barone, V.; Mennucci, B.; Petersson, G.; et al. *Gaussian 09*; Gaussian, Inc.: Wallingford, CT, 2009.

(28) Pham, C. V.; Mark, H. B.; Zimmer, H. *Synth. Commun.* **1986**, *16*, 689.

(29) Loewe, R. S.; Khersonsky, S. M.; McCullough, R. D. *Adv. Mater.* **1999**, *11*, 250.

(30) Loewe, R. S.; Ewbank, P. C.; Liu, J.; Zhai, L.; McCullough, R. D. *Macromolecules* **2001**, *34*, 4324.

(31) Boyd, S. D.; Jen, A. K. Y.; Luscombe, C. K. *Macromolecules* **2009**, *42*, 9387.

(32) Ho, V.; Boudouris, B. W.; Segalman, R. A. *Macromolecules* **2010**, *43*, 7895.

(33) Boudouris, B. W.; Ho, V.; Jimison, L. H.; Toney, M. F.; Salleo, A.; Segalman, R. A. *Macromolecules* **2011**, *44*, 6653.

DOI: 10.1021/jacs.5b02785
J. Am. Chem. Soc. 2015, 137, 6866−6879

(34) (a) Brown, P. J.; Thomas, D. S.; Köhler, A.; Wilson, J. S.; Kim, J.-S.; Ramsdale, C. M.; Sirringhaus, H.; Friend, R. H. *Phys. Rev. B* **2003**, *67*, No. 064203. (b) Hu, Z. J.; Adachi, T.; Haws, R.; Shuang, B.; Ono, R. J.; Bielawski, C. W.; Landes, C. F.; Rossky, P. J.; Vanden Bout, D. A. *J. Am. Chem. Soc.* **2014**, *136*, 16023.
(35) Burkhart, B.; Khlyabich, P. P.; Thompson, B. C. *Macromolecules* **2012**, *45*, 3740.
(36) (a) Clark, J.; Silva, C.; Friend, R. H.; Spano, F. C. *Phys. Rev. Lett.* **2007**, *98*, No. 206406. (b) Clark, J.; Chang, J.-F.; Spano, F. C.; Friend, R. H.; Silva, C. *Appl. Phys. Lett.* **2009**, *94*, No. 163306.
(37) Darling, S. B.; Sternberg, M. *J. Phys. Chem. B* **2009**, *113*, 6215.
(38) Salzner, U. *J. Phys. Chem. A* **2010**, *114*, 5397.
(39) (a) Tsoi, W. C.; James, D. T.; Kim, J. S.; Nicholson, P. G.; Murphy, C. E.; Bradley, D. D. C.; Nelson, J.; Kim, J.-S. *J. Am. Chem. Soc.* **2011**, *133*, 9834. (b) Tsoi, W. C.; James, D. T.; Domingo, E. B.; Kim, J. S.; Al-Hashimi, M.; Murphy, C. E.; Stingelin, N.; Heeney, M.; Kim, J.-S. *ACS Nano* **2012**, *6*, 9646.
(40) Raya, A.; Mora, M. A. *Polymer* **2004**, *45*, 6391.
(41) Garreau, S.; Leclerc, M.; Errien, N.; Louarn, G. *Macromolecules* **2003**, *36*, 692.
(42) (a) Pisula, W.; Menon, A.; Stepputat, M.; Lieberwirth, I.; Kolb, U.; Tracz, A.; Sirringhaus, H.; Pakula, T.; Mullen, K. *Adv. Mater.* **2005**, *17*, 684. (b) Duffy, C. M.; Andreasen, J. W.; Breiby, D. W.; Nielsen, M. M.; Ando, M.; Minakata, T.; Sirringhaus, H. *Chem. Mater.* **2008**, *20*, 7252. (c) James, D. T.; Frost, J. M.; Wade, J.; Nelson, J.; Kim, J. S. *ACS Nano* **2013**, *7*, 7983.
(43) (a) Zhang, X.; Bronstein, H.; Kronemeijer, A. J.; Smith, J.; Kim, Y.; Kline, R. J.; Richter, L. J.; Anthopoulos, T. D.; Sirringhaus, H.; Song, K.; Heeney, M.; Zhang, W.; McCulloch, I.; DeLongchamp, D. M. *Nat. Commun.* **2013**, *4*, 2238. (b) Fei, Z.; Pattanasattayavong, P.; Han, Y.; Schroeder, B. C.; Yan, F.; Kline, R. J.; Anthopoulos, T. D.; Heeney, M. *J. Am. Chem. Soc.* **2014**, *136*, 15154. (c) Noriega, R.; Rivnay, J.; Vandewal, K.; Koch, F. P. V.; Stingelin, N.; Smith, P.; Toney, M. F.; Salleo, A. *Nat. Mater.* **2013**, *12*, 1038. (d) Venkateshvaran, D.; Nikolka, M.; Sadhanala, A.; Lemaur, V.; Zelazny, M.; Kepa, M.; Hurhangee, M.; Kronemeijer, A. J.; Pecunia, V.; Nasrallah, I.; Romanov, I.; Broch, K.; McCulloch, I.; Emin, D.; Olivier, Y.; Cornil, J.; Beljonne, D.; Sirringhaus, H. *Nature* **2014**, *515*, 384.

DOI: 10.1021/jacs.5b02785
J. Am. Chem. Soc. 2015, 137, 6866−6879